

# Cosmological Constraints on 4D Einstein-Gauss-Bonnet Gravity and Kaniadakis Holographic Dark Energy: Implications for Black Hole Shadows

Xiang-Qian Li<sup>\*1</sup>, Hao-Peng Yan<sup>1</sup>, and Xiao-Jun Yue<sup>1</sup>

<sup>1</sup>College of Physics and Optoelectronic Engineering, Taiyuan University of Technology, Taiyuan 030024, China

December 1, 2025

## Abstract

The direct imaging of black holes by the Event Horizon Telescope (EHT) has inaugurated a new era of testing gravity in the strong-field regime. In this work, we investigate the cosmological evolution and optical appearance of black holes within the framework of 4D Einstein-Gauss-Bonnet (EGB) gravity coupled with Kaniadakis Holographic Dark Energy (KHDE). We perform a comprehensive study bridging cosmological scales to local astrophysical observables. First, utilizing the latest datasets from Cosmic Chronometers (CC) and Type Ia Supernovae (SNIa), we constrain the model parameters via Markov Chain Monte Carlo (MCMC) analysis. Our results indicate that the late-time universe statistically favors a phantom-like dark energy equation of state ( $w \approx 0.704$ ). Regarding the EGB coupling constant  $\alpha$ , although our data statistically favor a positive value, the parameter space permits negative values down to a sharp theoretical stability cut-off at  $\alpha \approx -0.03$ . Furthermore, while the best-fit value suggests a deviation, the results remain consistent with General Relativity ( $\alpha = 0$ ) within the  $2\sigma$  confidence level. Based on these constraints, we model the mass accretion history of supermassive black holes treating the accretion efficiency as a phenomenological constant, and compute the evolution of their shadow radius. We find that in a realistic dispersive plasma environment, the refractive effect significantly masks the intrinsic gravitational and dark energy signatures, causing a global shrinkage of the shadow. Nevertheless, a characteristic systematic intrinsic deviation of approximately 1%–1.5% (under this conservative accretion scenario) persists at low-to-intermediate redshifts ( $z \lesssim 1.5$ ) in the preferred parameter space relative to the standard  $\Lambda$ CDM prediction. Our findings suggest that while environmental effects dominate, precise statistical analyses of shadow populations could potentially disentangle these subtle dynamic dark energy signals from the standard cosmological paradigm.

## Contents

<b>1</b>	<b>Introduction</b>	<b>2</b>
<b>2</b>	<b>Theoretical Framework</b>	<b>3</b>
2.1	4D Einstein-Gauss-Bonnet Gravity	3
2.2	Kaniadakis Holographic Dark Energy (KHDE)	4
2.3	Modified Friedmann Equations	4
2.4	Black Hole Accretion Dynamics	4

---

<sup>\*</sup>Corresponding author: lixiangqian@tyut.edu.cn

<b>3</b>	<b>Observational Constraints</b>	<b>5</b>
3.1	Methodology and Datasets . . . . .	5
3.2	Results and Discussion . . . . .	6
<b>4</b>	<b>EoS Dynamics and Black Hole Mass Evolution</b>	<b>6</b>
4.1	Physical Scenarios . . . . .	7
4.2	Evolution of the Dark Energy Equation of State . . . . .	7
4.3	Black Hole Mass Accretion . . . . .	8
<b>5</b>	<b>Redshift Evolution of the Black Hole Shadow</b>	<b>9</b>
5.1	Photon Sphere and Shadow Radius in Optical Vacuum . . . . .	9
5.2	Intrinsic Evolution: The Impact of Phantom Crossing . . . . .	10
5.3	Impact of Plasma Environment . . . . .	11
5.3.1	The Dominance of Environmental Evolution . . . . .	13
5.3.2	Sensitivity to Accretion Profile . . . . .	14
<b>6</b>	<b>Conclusion and Discussion</b>	<b>14</b>

# 1 Introduction

The advent of the Event Horizon Telescope (EHT) has inaugurated a precision era for testing fundamental physics in the strong-field regime. The horizon-scale images of supermassive black holes M87\* [1] and Sagittarius A\* (Sgr A\*) [2] provide a unique opportunity to probe the spacetime geometry via the “black hole shadow.” While current observations remain consistent with General Relativity (GR), the measurement uncertainties leave ample room for alternative theories. This is particularly pertinent given the persistent challenges GR faces on cosmological scales, most notably the nature of dark energy and the initial singularity problem.

To address these cosmic puzzles, theoretical extensions often proceed by modifying either the gravitational action or the energy-momentum sector. In the gravitational sector, the 4D Einstein-Gauss-Bonnet (EGB) theory proposed by Glavan and Lin [3] has ignited intense research interest. By rescaling the Gauss-Bonnet coupling constant  $\alpha \rightarrow \alpha/(D-4)$  in the limit  $D \rightarrow 4$ , this theory bypasses the Lovelock theorem and admits non-trivial black hole solutions. Although the original regularization scheme faced criticism regarding its consistency [4, 5], subsequent well-defined scalar-tensor formulations [6, 7] have confirmed the validity of the resulting field equations for static spherically symmetric spacetimes. Extensive studies have since explored the phenomenological implications of 4D EGB gravity, including black hole thermodynamics [8–11], quasinormal modes [12–14], and notably, the optical properties of black hole shadows [15–18]. On cosmological scales, the theory allows for a negative coupling constant ( $\alpha < 0$ ), which can theoretically support non-singular “bouncing universe” solutions [19] and has been rigorously constrained by Big Bang Nucleosynthesis and late-time expansion data [20, 21].

Parallel to modifications of gravity, the dark energy sector has been enriched by the application of non-extensive statistical mechanics. Originating from the kinetic theory of particles, Kaniadakis ( $\kappa$ -) statistics [22, 23] offers a generalized entropy formalism that reduces to the standard Boltzmann-Gibbs entropy in the limit  $\kappa \rightarrow 0$ . Based on this framework, Kaniadakis Holographic Dark Energy (KHDE) was recently proposed as a microphysical basis for the accelerated expansion [24]. This model has demonstrated remarkable success in alleviating the  $H_0$  tension [25] and naturally accommodating the phantom-divide crossing ( $w < -1$ ) without invoking exotic matter fields [26, 27].

However, a critical disconnect remains between these global cosmological models and local astrophysical observables. Most studies on modified gravity black holes assume a static mass and

a vacuum environment, neglecting the dynamic interplay with the evolving Universe. In reality, black holes are embedded in a cosmological background and continuously interact with cosmic fluids. According to the Babichev model [28], a black hole immersed in a phantom dark energy fluid will lose mass over time, a phenomenon contrasting with standard accretion. Furthermore, astrophysical black holes are surrounded by dispersive plasma, whose density evolves with cosmic expansion ( $\rho \propto (1+z)^3$ ), significantly altering the shadow size via refractive effects [29, 30].

In this paper, we construct a unified framework to link the global cosmological evolution to the local shadow dynamics of 4D EGB black holes. Our investigation proceeds in three rigorous stages. First, we perform a Markov Chain Monte Carlo (MCMC) analysis using the latest Cosmic Chronometers (CC) and Type Ia Supernovae (SNIa) datasets to constrain the model parameters ( $H_0, \Omega_{m0}, \alpha, \beta, c$ ) without fixing the background to  $\Lambda$ CDM. Second, utilizing these observational constraints, we model the secular mass evolution of supermassive black holes driven by KHDE accretion, treating the accretion efficiency as a phenomenological parameter. Finally, we compute the redshift-dependent evolution of the black hole shadow radius, incorporating the metric corrections from 4D EGB gravity and the refractive masking effects of a cosmologically evolving plasma. Our primary objective is to assess whether the intrinsic signatures of modified gravity and phantom energy accretion persist as distinguishable statistical deviations beneath the dominant environmental signal of plasma refraction.

The remainder of this paper is organized as follows. Section 2 outlines the theoretical framework. Section 3 presents the observational constraints. Section 4 and Section 5 analyze the black hole mass evolution and shadow behavior, respectively. Finally, Section 6 summarizes our conclusions.

## 2 Theoretical Framework

In this section, we establish the theoretical foundations for our study. We first introduce the 4D Einstein-Gauss-Bonnet (EGB) gravity and its static spherically symmetric black hole solution. Subsequently, we outline the Kaniadakis Holographic Dark Energy (KHDE) model and derive the modified Friedmann equations governing the background cosmological evolution. Finally, we present the formalism for black hole mass accretion within this specific cosmological context.

### 2.1 4D Einstein-Gauss-Bonnet Gravity

The action for the Einstein-Gauss-Bonnet theory in  $D$ -dimensions is generally given by

$$S = \int d^D x \sqrt{-g} \left[ \frac{R}{16\pi G} + \alpha_{GB} \mathcal{G} + \mathcal{L}_m \right], \quad (1)$$

where  $R$  is the Ricci scalar,  $\mathcal{L}_m$  is the matter Lagrangian, and  $\mathcal{G} = R^2 - 4R_{\mu\nu}R^{\mu\nu} + R_{\mu\nu\rho\sigma}R^{\mu\nu\rho\sigma}$  is the Gauss-Bonnet invariant. While  $\mathcal{G}$  is a topological invariant in four dimensions, Glavan and Lin [3] proposed a regularization scheme by rescaling the coupling constant  $\alpha_{GB} \rightarrow \alpha/(D-4)$ . Taking the limit  $D \rightarrow 4$  at the level of field equations yields a set of non-trivial, diffeomorphism-invariant equations in 4D.

We consider a static, spherically symmetric spacetime ansatz  $ds^2 = -f(r)dt^2 + f(r)^{-1}dr^2 + r^2 d\Omega^2$ . Solving the modified vacuum field equations yields the metric function [3, 31]:

$$f(r) = 1 + \frac{r^2}{2\alpha} \left( 1 - \sqrt{1 + \frac{8\alpha M}{r^3}} \right), \quad (2)$$

where  $M$  is the geometric mass and  $\alpha$  is the rescaled EGB coupling constant (using geometric units  $G = c = 1$ ).

The sign of the coupling constant  $\alpha$  fundamentally dictates the spacetime structure. Positive values ( $\alpha > 0$ ) correspond to the standard branch asymptotically connected to General

Relativity. Conversely, the negative branch ( $\alpha < 0$ ) can describe a “bouncing universe” cosmology but imposes a strict stability condition: the metric function  $f(r)$  remains real only when  $1 + 8\alpha M/r^3 \geq 0$ . In the limit  $\alpha \rightarrow 0$ , expanding Eq. (2) recovers the standard Schwarzschild-de Sitter solution. This metric function serves as the background geometry for our shadow radius calculations.

## 2.2 Kaniadakis Holographic Dark Energy (KHDE)

The holographic dark energy hypothesis posits that the vacuum energy density  $\rho_{DE}$  scales with the infrared cutoff  $L$  (here  $L = H^{-1}$ ) and the horizon entropy. We adopt Kaniadakis statistics [22], which introduces a one-parameter generalization of the Boltzmann-Gibbs entropy,  $S_\kappa = \frac{1}{\beta} \sinh(\beta S_{BH})$ , where  $S_{BH} = \pi M_p^2 L^2$  is the standard Bekenstein-Hawking entropy and  $\beta$  quantifies non-extensive deviations.

Applying the holographic principle  $\rho_{DE} \propto S_\kappa L^{-4}$ , the energy density for KHDE takes the form [24]:

$$\rho_{DE} = 3H^2 M_p^2 \left( \frac{c^2}{y^2} + \frac{\beta^2 y^2}{3} \right), \quad (3)$$

where  $y \equiv LH = 1$  is the dimensionless Hubble horizon cutoff, and  $c$  is the model parameter determining the equation of state (EoS) at  $\beta = 0$ . Substituting Eq. (3) into the continuity equation  $\dot{\rho}_{DE} + 3H(1 + w_{DE})\rho_{DE} = 0$  yields the effective EoS parameter:

$$w_{DE}(z) = -1 - \frac{1+z}{3} \frac{d \ln \rho_{DE}}{dz}. \quad (4)$$

Depending on  $c$  and  $\beta$ ,  $w_{DE}(z)$  can exhibit rich dynamics, including the “phantom divide crossing” where the fluid transitions between quintessence ( $w > -1$ ) and phantom ( $w < -1$ ) phases.

## 2.3 Modified Friedmann Equations

We consider a flat Friedmann-Robertson-Walker (FRW) universe filled with pressureless matter ( $\rho_m$ ) and KHDE ( $\rho_{DE}$ ). In 4D EGB gravity, the expansion rate  $H \equiv \dot{a}/a$  is governed by a modified Friedmann equation containing an  $H^4$  correction term [19]:

$$H^2 + \alpha H^4 = \frac{8\pi G}{3}(\rho_m + \rho_{DE}). \quad (5)$$

Rewriting this in terms of the dimensionless Hubble parameter  $E(z) \equiv H(z)/H_0$  and density parameters  $\Omega_i$ , we obtain the physical branch of the expansion history:

$$E(z) = \sqrt{\frac{-1 + \sqrt{1 + 4\alpha[\Omega_{m0}(1+z)^3 + \Omega_{DE}(z)]}}{2\alpha}}. \quad (6)$$

The term under the inner square root imposes a stability bound,  $\Delta = 1 + 4\alpha\Omega_{tot}(z) \geq 0$ , ensuring the Hubble parameter remains real. This condition naturally provides a theoretical cut-off for negative  $\alpha$  values, which we will verify against observational data.

## 2.4 Black Hole Accretion Dynamics

To link the cosmological background to local black hole evolution, we employ the quasi-stationary accretion model proposed by Babichev et al. [28]. The secular mass evolution of a black hole immersed in a cosmic fluid is governed by the rate  $\dot{M} = 4\pi AM^2(\rho_{DE} + p_{DE})$ . Transforming the time derivative to redshift dependence using  $dt = -dz/[H(1+z)]$ , we arrive at the master equation:

$$\frac{dM}{dz} = -\frac{4\pi AM(z)^2 \rho_{DE}(z)[1 + w_{DE}(z)]}{H(z)(1+z)}. \quad (7)$$

Here,  $A$  is a dimensionless parameter characterizing the accretion efficiency. In rigorous hydrodynamic treatments, the exact value of  $A$  is typically determined via critical point analysis, where the fluid velocity matches the local sound speed at a specific sonic horizon [32, 33]. However, such an approach becomes ill-defined in the context of dynamical phantom-crossing models. As is characteristic of holographic dark energy scenarios, the squared sound speed  $c_s^2 = \partial p / \partial \rho$  exhibits divergences at the phantom divide ( $w \rightarrow -1$ ) and develops instabilities (negative values) in specific redshift ranges, rendering the standard sonic point condition  $u^2 = c_s^2$  physically unrealizable.

Consequently, we treat  $A$  as an effective phenomenological constant rather than a derived hydrodynamic quantity. We adopt a conservative value of  $4\pi A = 0.1$  in our numerical analysis to model a realistic, low-efficiency secular accretion scenario, which is consistent with observational constraints on quiescent supermassive black holes. Under this setup, the direction of mass evolution is strictly governed by the term  $(1 + w_{DE})$ . In the quintessence regime ( $w_{DE} > -1$ ),  $dM/dz < 0$ , implying the black hole mass grows as cosmic time progresses ( $z \rightarrow 0$ ). Conversely, in the phantom regime ( $w_{DE} < -1$ ), the condition  $dM/dz > 0$  implies a “negative accretion” process where the black hole loses mass over time (appearing more massive in the past). In the standard  $\Lambda$ CDM limit ( $w = -1$ ), the accretion rate vanishes, and the mass remains constant. We solve Eq. (7) numerically in Section 4 using the parameter constraints derived below.

### 3 Observational Constraints

To ensure the physical viability of our theoretical framework, we constrain the model parameters using a rigorous Bayesian statistical analysis. We employ the Markov Chain Monte Carlo (MCMC) method via the **Cobaya** sampling package [34], utilizing a customized likelihood module that implements the modified background evolution derived in Eq. (6). The total likelihood function is determined by  $\mathcal{L} \propto \exp(-\chi_{tot}^2/2)$ , where  $\chi_{tot}^2$  is the sum of the chi-squares from individual datasets.

#### 3.1 Methodology and Datasets

We analyze the parameter vector  $\Theta = \{H_0, \Omega_{m0}, \alpha, \beta, c\}$  assuming flat priors. Based on the configuration of our MCMC sampler, the specific prior ranges are chosen as follows:  $H_0 \in [50, 100] \text{ km s}^{-1} \text{ Mpc}^{-1}$ ,  $\Omega_{m0} \in [0.1, 0.7]$ ,  $\alpha \in [-0.15, 0.5]$ ,  $\beta \in [-1.0, 1.0]$ , and  $c \in [0.1, 3.0]$ . These wide ranges, particularly for the EGB coupling  $\alpha$  and the holographic parameter  $c$ , are adopted to avoid parameter railing and to fully explore the stability boundaries of the theory. Our analysis relies on two complementary late-time geometric probes that are independent of early-universe physics.

**Cosmic Chronometers (CC):** We utilize 31 measurements of the Hubble parameter  $H(z)$  obtained from the differential ages of passively evolving galaxies, covering the redshift range  $0.07 < z < 1.965$  [35]. These data provide direct constraints on the expansion rate  $E(z)$ . To evaluate the goodness of fit, we define the chi-square statistic for the CC dataset as:

$$\chi_{CC}^2 = \sum_{i=1}^{31} \left( \frac{H_{th}(z_i, \Theta) - H_{obs}(z_i)}{\sigma_{CC}(z_i)} \right)^2, \quad (8)$$

where  $H_{th}(z_i, \Theta)$  is the theoretical Hubble parameter predicted by our KHDE+EGB model, and  $H_{obs}(z_i) \pm \sigma_{CC}(z_i)$  represents the observed value and its standard uncertainty at redshift  $z_i$ .

**Type Ia Supernovae (SNIa):** We employ the Pantheon+ compilation [36], which consists of 1701 light curves of Type Ia supernovae spanning the redshift range  $0.001 < z < 2.26$ . The

theoretical distance modulus is given by:

$$\mu_{th}(z, \Theta) = 5 \log_{10} \left[ (1+z) \int_0^z \frac{dz'}{E(z', \Theta)} \right] + 25, \quad (9)$$

where  $E(z, \Theta) = H(z)/H_0$  is the dimensionless expansion rate. To assess the concordance between the model and the SNIa observations, we calculate the chi-square value using the full covariance matrix to account for systematic uncertainties:

$$\chi_{SNIa}^2 = \Delta\mu^T \cdot \mathbf{C}_{Pantheon+}^{-1} \cdot \Delta\mu. \quad (10)$$

Here,  $\mathbf{C}_{Pantheon+}$  is the covariance matrix of the Pantheon+ dataset, and  $\Delta\mu$  is the vector of residuals given by  $\Delta\mu_i = m_{B,i} - M - \mu_{th}(z_i, \Theta)$ , where  $m_{B,i}$  is the observed apparent magnitude and  $M$  is the absolute magnitude (treated as a nuisance parameter).

The total chi-square used in our joint analysis is the sum of the contributions from these two independent probes:

$$\chi_{tot}^2 = \chi_{CC}^2 + \chi_{SNIa}^2. \quad (11)$$

### 3.2 Results and Discussion

The joint posterior distributions and 2D confidence contours are presented in Figure 1, with detailed statistical summaries listed in Table 1.

Parameter	Symbol	Mean $\pm 1\sigma$	95% Confidence Interval
Hubble Constant	$H_0$	$73.634 \pm 4.151$	[66.733, 81.960]
Matter Density	$\Omega_{m0}$	$0.374 \pm 0.084$	[0.219, 0.537]
EGB Coupling	$\alpha$	$0.146 \pm 0.133$	[-0.030, 0.443]
Kaniadakis Parameter	$\beta$	$-0.005 \pm 0.495$	[-1.000, 1.000]
Holographic Parameter	$c$	$0.704 \pm 0.356$	[0.196, 1.449]

Table 1: Marginalized mean values and confidence limits for the model parameters constrained by CC + SNIa datasets.  $H_0$  is in units of  $\text{km s}^{-1} \text{Mpc}^{-1}$ .

The observational data reveal three critical physical insights. First, the holographic parameter prefers a value of  $c = 0.704 \pm 0.356$ . Since  $c < 1$  in HDE models corresponds to a phantom-like equation of state ( $w < -1$ ), this suggests the late-time universe is statistically dominated by phantom energy, although the quintessence regime is not ruled out at the  $2\sigma$  level. Second, the EGB coupling constant is constrained to  $\alpha = 0.146 \pm 0.133$ . Crucially, the 95% confidence interval exhibits a sharp lower cut-off at  $\alpha \approx -0.030$ . This empirical bound aligns perfectly with the theoretical stability condition of the theory (real-valued Hubble parameter), permitting a narrow window for the ‘‘bouncing universe’’ branch ( $\alpha < 0$ ) while favoring values consistent with General Relativity. Finally, the Kaniadakis parameter  $\beta$  remains unconstrained (mean  $-0.005 \pm 0.495$ ), indicating that background data alone cannot distinguish between extensive and non-extensive thermodynamics.

We also observe a strong degeneracy between  $\alpha$  and  $\Omega_{m0}$ , where a larger coupling constant compensates for higher matter density. Despite this, the best-fit model demonstrates excellent agreement with the observational data, as shown in Figure 2. Based on these results, we adopt the best-fit phantom scenario ( $c \approx 0.704$ ) as the baseline for our subsequent black hole analysis.

## 4 EoS Dynamics and Black Hole Mass Evolution

Having constrained the cosmological parameters in Section 3, we now apply these observational bounds to model the secular evolution of supermassive black holes. In the standard  $\Lambda$ CDM

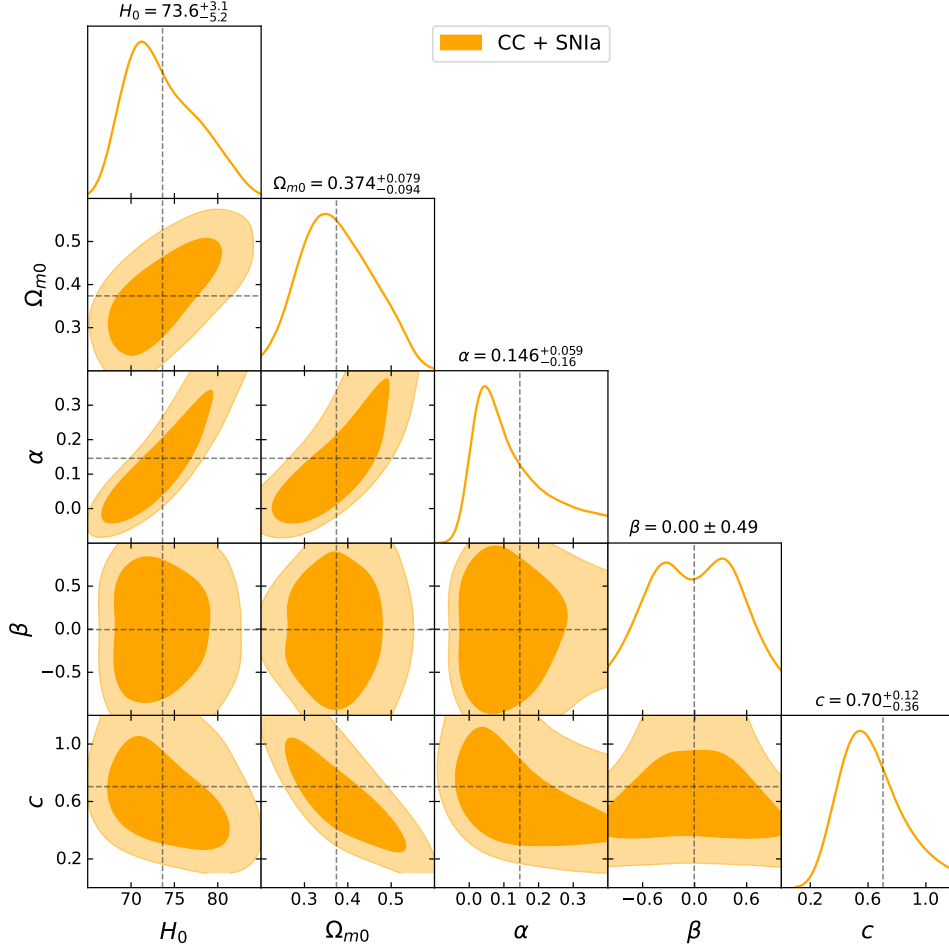


Figure 1: Confidence contours (68% and 95%) and 1D posterior distributions for the model parameters  $(H_0, \Omega_{m0}, \alpha, \beta, c)$  obtained from the joint analysis of CC + SNIa data. The grey dashed lines indicate the posterior means.

paradigm, the dark energy density is constant ( $w = -1$ ), leading to a static black hole mass ( $M(z) \equiv M_0$ ). In contrast, the KHDE framework predicts a redshift-dependent equation of state,  $w_{DE}(z)$ , which drives a dynamic mass accretion process governed by Eq. (7).

#### 4.1 Physical Scenarios

To systematically disentangle the effects of modified gravity from those of non-extensive thermodynamics, we define seven physical scenarios based on the posterior mean values derived from our MCMC analysis ( $H_0 = 73.6$ ,  $\Omega_{m0} = 0.37$ ,  $c = 0.70$ ). These scenarios are detailed in Table 2. They are categorized into two groups: “Group A” assumes standard Bekenstein-Hawking entropy ( $\beta = 0$ ) to isolate the effects of EGB gravity, while “Group B” incorporates Kaniadakis non-extensive statistics ( $\beta = 0.5$ ).

#### 4.2 Evolution of the Dark Energy Equation of State

The black hole accretion rate,  $\dot{M}$ , is critically sensitive to the term  $(1+w_{DE})$ . Figure 3 illustrates the redshift evolution of the equation of state parameter,  $w_{DE}(z)$ , for the selected scenarios. A defining characteristic of the KHDE model is the dynamic crossing of the “Phantom Divide” ( $w = -1$ ). In the local universe ( $z \lesssim 0.25$ ), the equation of state exhibits phantom behavior ( $w < -1$ ), which is consistent with our best-fit holographic parameter  $c \approx 0.70$ . As we look



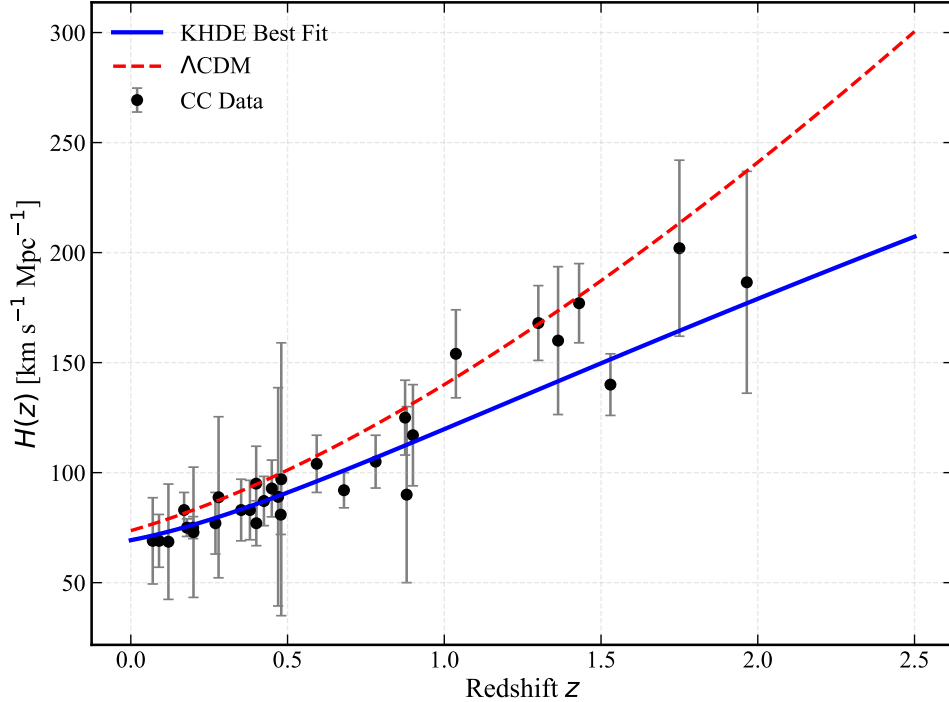


Figure 2: The Hubble parameter  $H(z)$  as a function of redshift. The blue solid line represents the best-fit KHDE model ( $H_0 = 73.6, c = 0.70, \alpha = 0.146$ ), demonstrating strong agreement with the Cosmic Chronometers data (black dots).

back to higher redshifts, the fluid transitions into the quintessence regime ( $w > -1$ ). The EGB coupling  $\alpha$  modulates this trajectory, with positive  $\alpha$  suppressing the high-redshift value of  $w_{DE}$  relative to General Relativity, and negative  $\alpha$  enhancing it.

### 4.3 Black Hole Mass Accretion

The impact of the evolving dark energy background on the black hole mass is presented in Figure 4. The evolution curves reveal a rich dynamical structure governed by the interplay of phantom crossing, modified gravity, and non-extensive thermodynamics. The most prominent feature shared by all KHDE scenarios is the distinctive “hump” shape of the mass evolution curves, which serves as a dynamical fingerprint of the phantom divide crossing. In the low-redshift regime ( $z \lesssim 0.25$ ), where the dark energy is phantom-like ( $w_{DE} < -1$ ), the accretion rate becomes negative. Physically, this corresponds to a phase where the black hole loses mass as cosmic time progresses forward (or equivalently, appears more massive in the past), driving the upward slope from  $z = 0$ . Conversely, at higher redshifts ( $z \gtrsim 0.25$ ), the universe transitions into the quintessence phase ( $w_{DE} > -1$ ), restoring the normal accretion regime where mass grows over time (decreases with redshift). The peak of the mass distribution thus precisely marks the phantom crossing epoch where  $1 + w_{DE} = 0$ .

Beyond this global non-monotonic trend, the trajectories exhibit a clear vertical stratification driven by the EGB coupling constant  $\alpha$ . It is important to emphasize that, since we adopt a fixed accretion parameter  $A$  across all scenarios, this stratification arises purely from the cosmological modification of the background expansion rate  $H(z)$  and the dark energy density  $\rho_{DE}(z)$ , rather than from local hydrodynamic corrections to the accretion flow. Specifically, the curves associated with negative  $\alpha$  (Red/Purple) exhibit the largest deviation from the GR baseline. A negative coupling modifies the Friedmann equation to effectively enhance the expansion rate and the dark energy density terms; thus, even with a constant accretion efficiency, the effective mass



Table 2: Definition of the seven physical scenarios investigated in this work. The background cosmological parameters are fixed to the MCMC posterior means. The scenarios are categorized by their entropy definition and gravitational coupling.

Scenario	$\beta$	$\alpha$	Physical Interpretation
<b>Reference Model</b>			
Standard $\Lambda$ CDM	–	0	Standard cosmological constant ( $w = -1$ , const. mass).
<b>Group A: Standard Bekenstein-Hawking Entropy (<math>\beta = 0</math>)</b>			
BH-GR	0	0	Baseline KHDE phantom model in GR.
BH-EGB(–)	0	–0.005	Bouncing universe branch.
BH-EGB(+)	0	+0.146	Non-bouncing universe branch.
<b>Group B: Kaniadakis Non-Extensive Entropy (<math>\beta = 0.5</math>)</b>			
Kaniadakis-GR	0.5	0	Pure non-extensive statistical correction.
Kaniadakis-EGB(–)	0.5	–0.005	Combined non-extensive and bouncing effects.
Kaniadakis-EGB(+)	0.5	+0.146	Combined non-extensive and non-bouncing effects.

growth rate is amplified due to the denser cosmic background. In contrast, trajectories with positive  $\alpha$  (Orange/Brown) lie closer to the standard  $\Lambda$ CDM limit, as the positive coupling tends to suppress the dynamic range of the equation of state, resulting in a milder secular evolution.

Finally, within each gravitational bundle, we observe a secondary splitting induced by the Kaniadakis entropy parameter  $\beta$ . By comparing the standard entropy models ( $\beta = 0$ , solid/dashed lines) with the Kaniadakis models ( $\beta = 0.5$ , dot-dashed lines), it becomes evident that non-extensive statistics introduce a subtle but systematic shift in the mass curves. This effect arises because a non-zero  $\beta$  fundamentally modifies the holographic dark energy density and its equation of state (as defined in Eq. 3), slightly shifting the timing of the phantom crossing. Although sub-dominant compared to the gravitational  $\alpha$ -effect, this thermodynamic correction confirms that the microphysics of the dark energy sector leaves a distinguishable imprint on the macroscopic evolution of black holes through the modulation of the cosmic energy reservoir.

## 5 Redshift Evolution of the Black Hole Shadow

The observable shadow of a black hole is characterized by the critical impact parameter of photons that can escape to infinity. This characteristic size depends on two distinct factors: the intrinsic geometry of the spacetime—determined by the evolving black hole mass  $M(z)$  and the EGB coupling  $\alpha$ —and the propagation of light rays through the intervening cosmic medium. In this section, we first analyze the shadow evolution in an optical vacuum to isolate the effects of modified gravity and mass accretion, before investigating the realistic scenario incorporating plasma refraction.

### 5.1 Photon Sphere and Shadow Radius in Optical Vacuum

For a static observer at infinity, the effective potential  $V_{eff}(r)$  for photons moving in the equatorial plane of the 4D EGB metric is given by  $V_{eff}(r) = f(r)L^2/r^2$ , where  $L$  is the photon angular momentum. The radius of the unstable photon sphere,  $r_{ph}$ , is determined by the condition  $V'_{eff}(r_{ph}) = 0$ , yielding the equation:

$$2f(r_{ph}) - r_{ph}f'(r_{ph}) = 0. \quad (12)$$

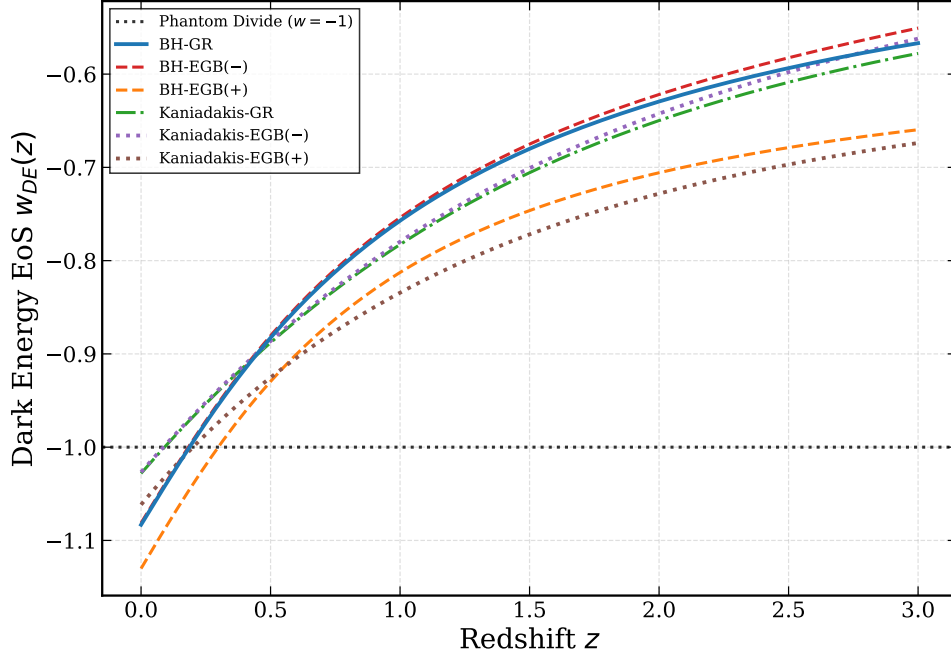


Figure 3: Evolution of the dark energy equation of state  $w_{DE}(z)$ . The horizontal dotted line represents the Phantom Divide ( $w = -1$ ). All KHDE models exhibit a dynamical crossing: a phantom phase ( $w < -1$ ) at low redshifts ( $z \lesssim 0.25$ ) and a quintessence phase ( $w > -1$ ) at higher redshifts.

While the standard Schwarzschild limit ( $\alpha = 0$ ) yields  $r_{ph} = 3M$ , the 4D EGB solution introduces an  $\alpha$ -dependence. The observable shadow radius  $R_{sh}$  corresponds to the critical impact parameter:

$$R_{sh} = \frac{r_{ph}}{\sqrt{f(r_{ph})}}. \quad (13)$$

## 5.2 Intrinsic Evolution: The Impact of Phantom Crossing

To disentangle geometric effects from environmental factors, we first examine the shadow evolution in an optical vacuum ( $n = 1$ ). Figure 5 presents the evolution of the normalized shadow radius  $R_{sh}(z)/M_0$  for the seven scenarios defined in Table 2.

The evolution of the shadow radius exhibits a morphology that is intrinsically linked to the mass accretion history analyzed in Section 4, yet it reveals how spacetime geometry modulates observable signatures. The non-monotonic “hump” feature—rising in the low-redshift phantom domain ( $z \lesssim 0.25$ ) and falling in the high-redshift quintessence domain ( $z \gtrsim 0.25$ )—is a direct geometric mapping of the mass evolution profile  $M(z)$ . This confirms that in an optical vacuum, the shadow radius acts as a faithful tracer of the dark energy equation of state, preserving the dynamical fingerprint of the phantom crossing.

However, the translation from mass to shadow size involves a critical geometric factor governed by the EGB gravitational coupling  $\alpha$ . We observe the same vertical stratification as in the mass sector, but with a distinct physical origin. While the *shape* of the curves is dictated by the accretion history (under a fixed efficiency parameter  $A$ ), the *absolute scaling* is dominated by the direct modification of the photon sphere radius  $r_{ph}$  in the EGB metric. Specifically, the negative  $\alpha$  branch (Red/Purple) effectively weakens the gravitational potential in the strong-field regime, pushing the photon sphere outward and enlarging the shadow relative to GR. Conversely, positive  $\alpha$  (Orange/Brown) compresses the shadow. This implies that EGB gravity breaks the degeneracy between accretion and geometry: it introduces a static geometric offset that persists

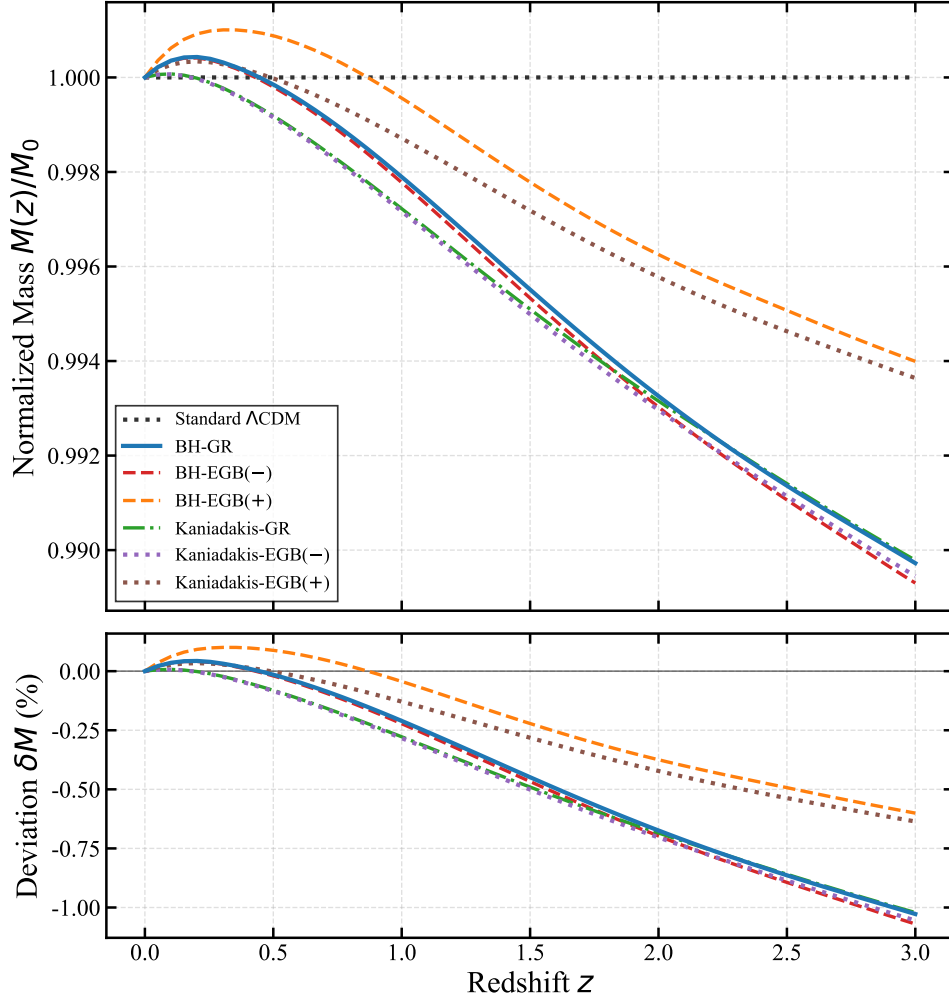


Figure 4: Evolution of the normalized black hole mass  $M(z)/M_0$ . The curves exhibit a non-monotonic behavior mirroring the EoS dynamics: mass increases with redshift in the local phantom regime ( $z \lesssim 0.25$ ) due to negative accretion, and decreases in the high-redshift quintessence regime.

across cosmic time, shifting the baseline of the accretion-driven curve independent of the fluid dynamics.

Finally, the thermodynamic fine-tuning observed in the mass sector propagates into the shadow sector. Within each gravitational bundle, the Kaniadakis entropy ( $\beta = 0.5$ ) induces a secondary splitting in the shadow radius. Although this effect is subtler than the geometric  $\alpha$ -shift, it demonstrates that the microphysical properties of the dark energy fluid—by modulating the background expansion and accretion rate—leave a distinguishable imprint on the strong-field optical appearance of the black hole.

### 5.3 Impact of Plasma Environment

In realistic astrophysical contexts, black holes are not isolated in a vacuum but are surrounded by dispersive plasma. The presence of this medium introduces a frequency-dependent refractive index  $n$ , which modifies the photon trajectories and consequently alters the observable shadow size. Crucially, in a cosmological framework, the properties of this environment are not static; they evolve with the expansion of the Universe.

We model the accretion environment as a cold, non-magnetized, dispersive plasma. The

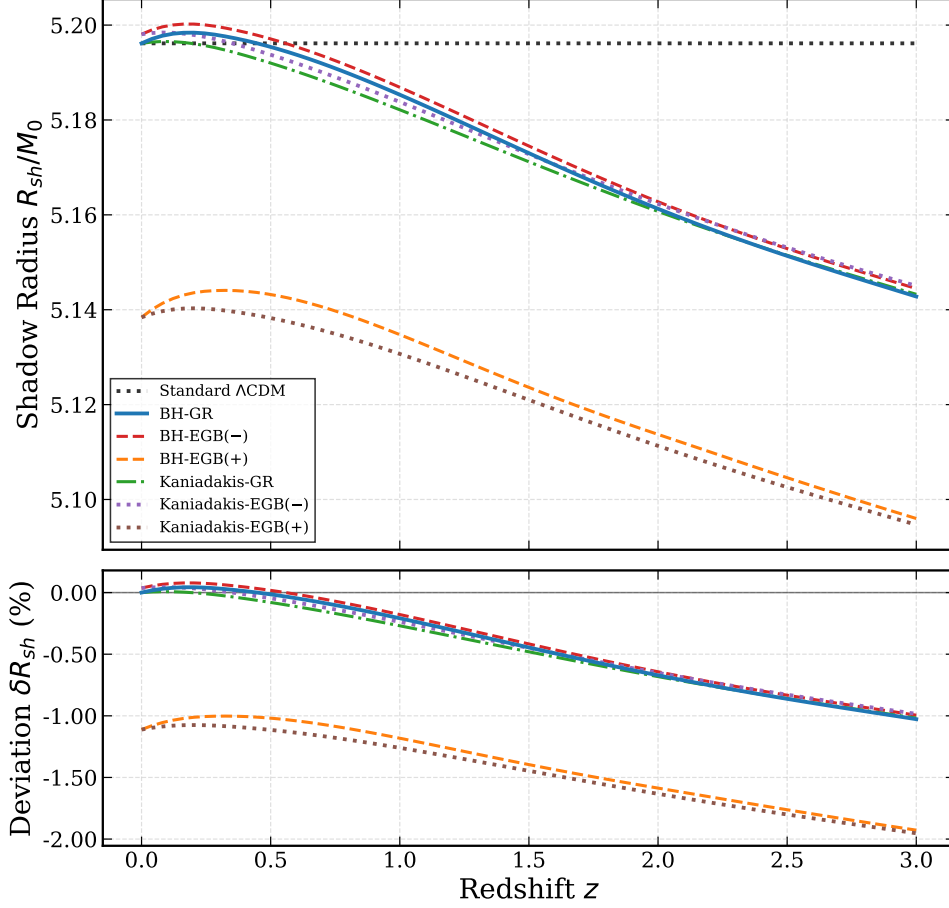


Figure 5: Evolution of the black hole shadow radius in an optical vacuum ( $n = 1$ ) for the seven physical scenarios. The black dotted line represents the standard  $\Lambda$ CDM prediction. The colored curves exhibit a non-monotonic “hump” shape—rising at low redshifts ( $z \lesssim 0.25$ ) and falling at high redshifts ( $z > 0.25$ )—which mirrors the mass evolution driven by the phantom-divide crossing. The vertical stratification is governed by the EGB coupling  $\alpha$ .

refractive index  $n$  for a photon with angular frequency  $\omega(r)$  propagating through this medium is governed by the dispersion relation:

$$n^2 = 1 - \frac{\omega_p(r)^2}{\omega(r)^2}. \quad (14)$$

Here,  $\omega_p(r)$  is the electron plasma frequency, defined by  $\omega_p^2 = 4\pi e^2 N_e(r)/m_e$ , where  $e$  is the electron charge,  $m_e$  is the electron mass, and  $N_e(r)$  is the electron number density [29]. The term  $\omega(r)$  represents the photon frequency measured by a local static observer. The physical significance of this relation is that the plasma acts as a dispersive medium where the phase velocity exceeds the speed of light ( $n < 1$ ), leading to the refraction of light rays away from the high-density region.

To link this local physics to global cosmological evolution, we incorporate two competing redshift-dependent effects:

1. **Density Evolution ( $\omega_p$  term):** We assume the local plasma density surrounding the black hole scales with the cosmic expansion history. Since the average matter density of the Universe evolves as  $\rho \propto (1+z)^3$ , we impose a similar scaling on the plasma number density:  $N_e(z) \propto (1+z)^3$ . Consequently, the plasma frequency squared scales as  $\omega_p^2(z) \propto (1+z)^3$ .

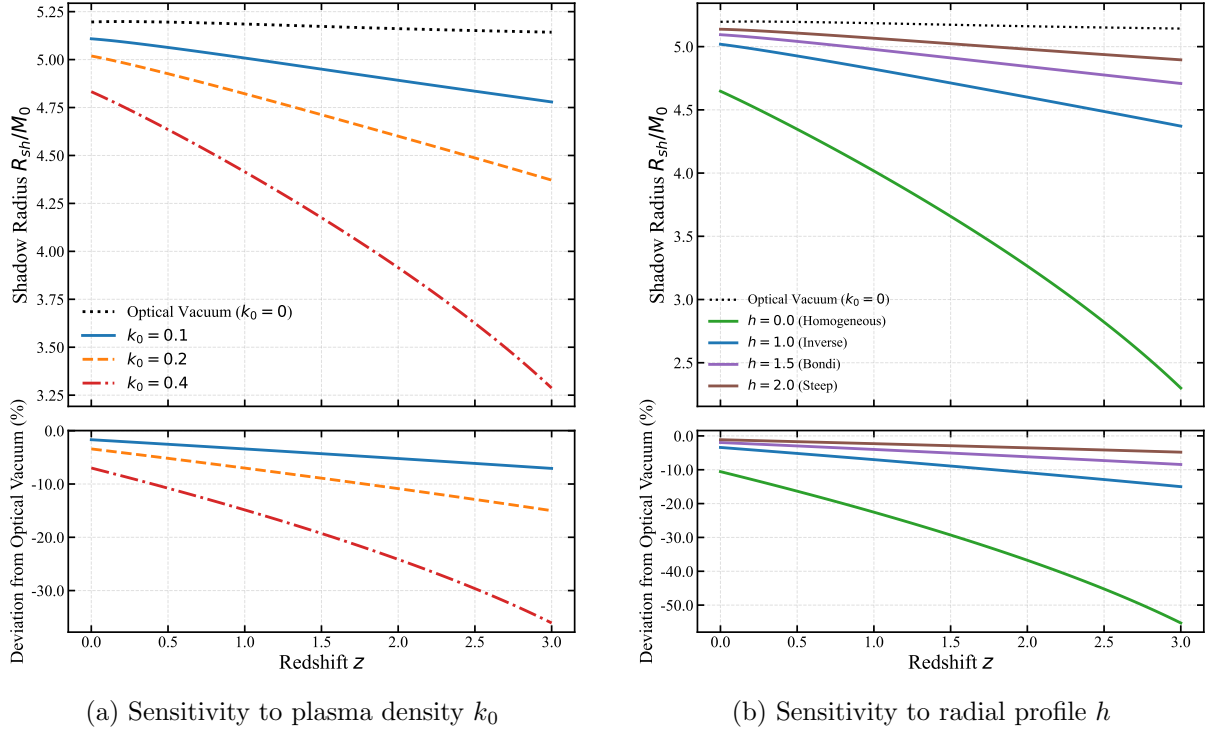


Figure 6: **Impact of Plasma Environment.** (a) Comparison of shadow evolution in optical vacuum ( $k_0 = 0$ ) versus dispersive plasma ( $k_0 > 0$ ) for fixed  $h = 1$ . (b) Sensitivity to the radial profile slope  $h$  for fixed density  $k_0 = 0.2$ . The baseline model is Bekenstein-Hawking-GR.

2. **Frequency Redshift ( $\omega$  term):** Due to the cosmic expansion, the photon frequency  $\omega$  observed at a high redshift  $z$  relates to the observed frequency  $\omega_0$  at  $z = 0$  via the standard relation  $\omega(z) = \omega_0(1 + z)$ . Squaring this gives  $\omega^2(z) \propto (1 + z)^2$ .

Combining these factors, the ratio governing the refractive strength evolves linearly with redshift:

$$\frac{\omega_p^2(z)}{\omega^2(z)} \propto \frac{(1 + z)^3}{(1 + z)^2} = (1 + z). \quad (15)$$

By further assuming a power-law radial density profile  $N_e(r) \propto r^{-h}$  to describe the accretion geometry, we arrive at the parameterized effective refractive index profile used in our simulation:

$$n(r, z) = \sqrt{1 - \frac{k_0(1 + z)}{r^h}}, \quad (16)$$

where  $h$  determines the steepness of the radial density fall-off, and  $k_0$  is a dimensionless constant characterizing the normalized plasma density at the present epoch ( $z = 0$ ). Under this framework, the observable shadow radius is modified to  $R_{sh}(z) = r_{ph}n(r_{ph}, z)/\sqrt{f(r_{ph})}$ . Since the term  $\frac{k_0(1+z)}{r^h}$  increases with redshift, the refractive index  $n$  decreases, causing the plasma to act as a progressively stronger diverging lens in the early universe.

### 5.3.1 The Dominance of Environmental Evolution

The interplay between intrinsic mass growth and environmental screening is analyzed in Figure 6(a), where we compare the vacuum case ( $k_0 = 0$ , red curve) against the plasma case ( $k_0 = 0.2$ , blue curve). This comparison reveals a dramatic inversion of the evolutionary trend. In the optical vacuum, the shadow radius increases with redshift, reflecting the intrinsic mass growth driven by phantom energy accretion. However, in the presence of plasma, the curve exhibits a

negative slope. Despite the black hole being physically more massive in the past (a consequence of the  $w < -1$  equation of state), the plasma density scales as  $(1+z)^3$ , which significantly reduces the refractive index at high redshifts. This “environmental screening” effect completely overpowers the intrinsic mass accretion signal, causing the observable shadow to appear smaller at higher redshifts. This finding highlights a critical observational degeneracy: a shrinking shadow at high  $z$  is not necessarily evidence of quintessence accretion (normal mass growth) but is more likely a signature of the evolving cosmic medium.

### 5.3.2 Sensitivity to Accretion Profile

To verify the robustness of these results, we examine the sensitivity to the radial profile parameter  $h$  in Figure 6(b). While steeper density profiles (e.g., Bondi accretion,  $h = 1.5$ ) result in larger absolute shadow sizes due to the rapid density drop-off away from the horizon, the qualitative trend remains unchanged. For all physically motivated values of  $h$ , the shadow size decreases with redshift ( $dR_{sh}/dz < 0$ ). This confirms that the global cosmological evolution of the background density is the primary driver of the shadow’s redshift dependence, rendering the specific details of the local accretion geometry a second-order effect.

## 6 Conclusion and Discussion

In this work, we have constructed a unified framework to bridge the gap between global cosmological expansion and local strong-field astrophysics. By immersing 4D Einstein-Gauss-Bonnet (EGB) black holes in a Kaniadakis Holographic Dark Energy (KHDE) cosmology, we explored how the interplay of modified gravity, dynamic dark energy accretion, and plasma environments shapes the observable properties of supermassive black holes.

Our investigation began with a rigorous MCMC analysis of the background cosmology using Cosmic Chronometers and Type Ia Supernovae. The data statistically favor a phantom-like equation of state for the KHDE model ( $c = 0.704 \pm 0.356$ ), suggesting that the late-time universe is dominated by a fluid with  $w < -1$ . Regarding the gravitational sector, the EGB coupling constant is constrained to  $\alpha = 0.146 \pm 0.133$ . Crucially, we identified a strict empirical lower bound at  $\alpha \approx -0.030$ , which aligns with the theoretical stability condition required for a real-valued Hubble parameter. This result permits the “bouncing universe” branch ( $\alpha < 0$ ) only within a narrow window close to General Relativity.

Building on these constraints, we modeled the secular evolution of supermassive black holes under the assumption of a constant effective accretion efficiency ( $4\pi A = 0.1$ ). We found that the preferred phantom cosmology induces a “negative accretion” process, implying that black holes were effectively more massive in the past. This leads to a non-monotonic evolution of the shadow radius in an optical vacuum: the shadow size initially increases with redshift, peaks at the phantom crossing point ( $z \approx 0.25$ ), and then decreases. While the magnitude of this evolution scales with the accretion parameter  $A$ , the morphological trend is robustly determined by the dark energy equation of state. Furthermore, the EGB coupling  $\alpha$  introduces a vertical stratification in the shadow size, thereby breaking the degeneracy between mass accretion history and gravitational geometry.

However, the inclusion of a realistic dispersive plasma environment fundamentally alters this picture. Our analysis reveals that the cosmological evolution of the plasma density ( $\rho_{plasma} \propto (1+z)^3$ ) acts as the dominant factor determining the shadow’s optical appearance. The increasing plasma density at high redshifts suppresses the refractive index, creating a diverging lens effect that overpowers the intrinsic phantom mass growth regardless of the specific accretion efficiency. Consequently, the absolute shadow size is observed to shrink with redshift, inverting the trend predicted by vacuum models.

Despite this global shrinkage caused by the environment, our model predicts a distinct observational signature that persists beneath the noise. The signature of phantom accretion manifests

not as a temporal evolution of a single object, but as a *statistical deviation* from the standard mass-shadow scaling relation across the cosmic population. Specifically, contrary to the static  $\Lambda$ CDM prediction, our KHDE+EGB model predicts a systematic **intrinsic reduction** in the shadow size at high redshifts. Under our conservative accretion scenario, this manifests at  $z \approx 2.5$  as a deviation of approximately  $-1\%$  to  $-1.5\%$  (depending on the gravitational coupling  $\alpha$ ) relative to the standard vacuum prediction. While the refractive effect (causing  $\sim 10\%$ – $15\%$  shrinkage) creates a significant observational challenge by masking this subtle intrinsic signal, the redshift-dependent refractive scaling serves as a predictable “cosmological baseline.” We conclude that by statistically stacking shadow measurements from multiple sources in redshift bins to average out local environmental variations, future high-precision surveys may potentially uncover this elusive systematic anomaly, thereby offering a novel probe of dynamic dark energy in the strong-gravity regime.

## Acknowledgments

This work was supported by the National Natural Science Foundation of China under Grant No. 12305070, and the Basic Research Program of Shanxi Province under Grant Nos. 202303021222018 and 202303021221033.

## References

- [1] Event Horizon Telescope Collaboration. First m87 event horizon telescope results. i. the shadow of the supermassive black hole. *Astrophys. J. Lett.*, 875:L1, 2019.
- [2] Event Horizon Telescope Collaboration. First sagittarius a\* event horizon telescope results. i. the shadow of the supermassive black hole in the center of the milky way. *Astrophys. J. Lett.*, 930:L12, 2022.
- [3] D. Glavan and C. Lin. Einstein-gauss-bonnet gravity in four-dimensional spacetime. *Phys. Rev. Lett.*, 124:081301, 2020.
- [4] H. Lu and Yi Pang. Horndeski gravity as  $D \rightarrow 4$  limit of Gauss-Bonnet. *Phys. Lett. B*, 809:135717, 2020.
- [5] Wen-Yuan Ai. A note on the novel 4D Einstein–Gauss–Bonnet gravity. *Commun. Theor. Phys.*, 72(9):095402, 2020.
- [6] Robie A. Hennigar, David Kubizňák, Robert B. Mann, and Christopher Pollack. On taking the  $D \rightarrow 4$  limit of Gauss-Bonnet gravity: theory and solutions. *JHEP*, 07:027, 2020.
- [7] Pedro G. S. Fernandes. Charged black holes in AdS spaces in 4D Einstein Gauss-Bonnet gravity. *Phys. Lett. B*, 805:135468, 2020.
- [8] Shao-Wen Wei and Yu-Xiao Liu. Extended thermodynamics and microstructures of four-dimensional charged Gauss-Bonnet black hole in AdS space. *Phys. Rev. D*, 101(10):104018, 2020.
- [9] Kartheek Hegde, A. Naveena Kumara, C. L. Ahmed Rizwan, Md Sabir Ali, and K. M. Ajith. Null geodesics and thermodynamic phase transition of four-dimensional Gauss–Bonnet AdS black hole. *Annals Phys.*, 429:168461, 2021.
- [10] Indrajit Halder. Thermodynamics and circular motion in a 4D Einstein–Gauss–Bonnet black hole embedded in quintessence. *Can. J. Phys.*, 103(10):978–992, 2025.



- [11] Xiao-yan Hu, Yuan-zhang Cui, and Wei Xu. Hawking-Page transition in 4D Einstein-Gauss-Bonnet gravity. *Nucl. Phys. B*, 1012:116821, 2025.
- [12] M. S. Churilova. Quasinormal modes of the test fields in the consistent 4D Einstein-Gauss-Bonnet-(anti)de Sitter gravity. *Annals Phys.*, 427:168425, 2021.
- [13] R. A. Konoplya and A. F. Zinhailo. Quasinormal modes, stability and shadows of a black hole in the 4D Einstein-Gauss-Bonnet gravity. *Eur. Phys. J. C*, 80(11):1049, 2020.
- [14] Ramón Bécar, P. A. González, Eleftherios Papantonopoulos, and Yerko Vásquez. Massive scalar field perturbations of 4D de Sitter-Einstein-Gauss-Bonnet black holes. *Phys. Rev. D*, 111(12):124013, 2025.
- [15] M. Zubair, Muhammad Ali Raza, Furkat Sarikulov, and Javlon Rayimbaev. 4D Einstein-Gauss-Bonnet black hole in Power-Yang-Mills field: a shadow study. *JCAP*, 10:058, 2023.
- [16] Javier Badía and Ernesto F. Eiroa. Shadow of black holes with a plasma environment in 4D Einstein-Gauss-Bonnet gravity. In *16th Marcel Grossmann Meeting on Recent Developments in Theoretical and Experimental General Relativity, Astrophysics and Relativistic Field Theories*, 11 2021.
- [17] R. Kumar and S. G. Ghosh. Rotating black holes in 4d einstein-gauss-bonnet gravity and its shadow. *JCAP*, 07:053, 2020.
- [18] Tian-Tian Liu, He-Xu Zhang, Yu-Hang Feng, Jian-Bo Deng, and Xian-Ru Hu. Double shadow of a 4D Einstein-Gauss-Bonnet black hole and the connection between them with quasinormal modes. *Mod. Phys. Lett. A*, 37(24):2250154, 2022.
- [19] H. Khodabakhshi, M. Farhang, and H. Lü. Observational feasibility of 4D Einstein-Gauss-Bonnet cosmology: bouncing and non-bouncing universes. *JCAP*, 05:024, 2024.
- [20] Carola M. A. Zanoletti, Brayden R. Hull, C. Danielle Leonard, and Robert B. Mann. Cosmological constraints on 4-dimensional Einstein-Gauss-Bonnet gravity. *JCAP*, 01:043, 2024.
- [21] Timothy Clifton, Pedro Carrilho, Pedro GS Fernandes, and David J Mulryne. Observational constraints on the regularized 4d einstein-gauss-bonnet theory of gravity. *Phys. Rev. D*, 102(8):084058, 2020.
- [22] G. Kaniadakis. Statistical mechanics in the context of special relativity. *Phys. Rev. E*, 66:056125, 2002.
- [23] Giorgio Kaniadakis. Statistical mechanics in the context of special relativity. ii. *Phys. Rev. E*, 72(3):036108, 2005.
- [24] Niki Drepanou, Andreas Lymperis, Emmanuel N. Saridakis, and Kuralay Yesmakhanova. Kaniadakis holographic dark energy and cosmology. *Eur. Phys. J. C*, 82(5):449, 2022.
- [25] A. Hernández-Almada, Genly Leon, Juan Magaña, Miguel A. García-Aspeitia, V. Motta, Emmanuel N. Saridakis, and Kuralay Yesmakhanova. Kaniadakis-holographic dark energy: observational constraints and global dynamics. *Mon. Not. Roy. Astron. Soc.*, 511(3):4147–4158, 2022.
- [26] Xiaofang Shen, Bing Xu, Kaituo Zhang, Xiangyun Fu, Liangliang Ren, and Zelin Zhang. Revisiting the constraints on interacting holographic dark energy models with current observational data. *Eur. Phys. J. C*, 85(9):992, 2025.

- [27] Andreas Lymperis, Spyros Basilakos, and Emmanuel N. Saridakis. Modified cosmology through Kaniadakis horizon entropy. *Eur. Phys. J. C*, 81(11):1037, 2021.
- [28] E. Babichev, V. Dokuchaev, and Y. Eroshenko. Black hole mass decreasing due to phantom energy accretion. *Phys. Rev. Lett.*, 93:021102, 2004.
- [29] V. Perlick, O. Y. Tsupko, and G. S. Bisnovatyi-Kogan. Influence of a plasma on the shadow of a spherically symmetric black hole. *Phys. Rev. D*, 92:104031, 2015.
- [30] Mou Xu, Ruonan Li, Jianbo Lu, Shining Yang, and Shu-Min Wu. Optical appearance and shadow of Kalb–Ramond black hole: effects of plasma and accretion models. *Eur. Phys. J. C*, 85(6):676, 2025.
- [31] P. G. S. Fernandes, P. Carrilho, T. Clifton, and D. J. Mulryne. The 4d einstein-gauss-bonnet theory of gravity: a review. *Class. Quant. Grav.*, 39:063001, 2022.
- [32] P. Mukherjee, U. Debnath, H. Chaudhary, and G. Mustafa. Constraining the parameters of generalized and viscous modified chaplygin gas and black hole accretion in einstein-aether gravity. *Eur. Phys. J. C*, 84:930, 2024.
- [33] Ritabrata Biswas, Nairwita Mazumder, and Subenoy Chakraborty. Accretion of Holographic Dark Energy : Dependency only upon Horizon Radius of Expanding Universe. *Astrophys. Space Sci.*, 335:603–609, 2011.
- [34] J. Torrado and A. Lewis. Cobaya: Code for bayesian analysis of hierarchical physical models. *J. Cosmol. Astropart. Phys.*, 2021(05):057, 2021.
- [35] M. Moresco and et al. A 6% measurement of the hubble parameter at  $z \sim 0.45$ : direct evidence of the epoch of cosmic re-acceleration. *J. Cosmol. Astropart. Phys.*, 2016(05):014, 2016.
- [36] D. Brout et al. The pantheon+ analysis: Cosmological constraints. *Astrophys. J.*, 938:110, 2022.